scientific reports

Check for updates

OPEN

The non-volatile electrostatic doping effect in $MoTe_2$ field-effect transistors controlled by hexagonal boron nitride and a metal gate

Muhammad Asghar Khan[1,4], Muhammad Farooq Khan[2,4], Shania Rehman[2,3], Harshada Patil[2,3], Ghulam Dastgeer[1], Byung Min Ko[1] & Jonghwa Eom[1]✉

The electrical and optical properties of transition metal dichalcogenides (TMDs) can be effectively modulated by tuning their Fermi levels. To develop a carrier-selectable optoelectronic device, we investigated intrinsically p-type $MoTe_2$, which can be changed to n-type by charging a hexagonal boron nitride (h-BN) substrate through the application of a writing voltage using a metal gate under deep ultraviolet light. The n-type part of $MoTe_2$ can be obtained locally using the metal gate pattern, whereas the other parts remain p-type. Furthermore, we can control the transition rate to n-type by applying a different writing voltage (i.e., − 2 to − 10 V), where the n-type characteristics become saturated beyond a certain writing voltage. Thus, $MoTe_2$ was electrostatically doped by a charged h-BN substrate, and it was found that a thicker h-BN substrate was more efficiently photocharged than a thinner one. We also fabricated a p–n diode using a 0.8 nm-thick $MoTe_2$ flake on a 167 nm-thick h-BN substrate, which showed a high rectification ratio of ~ 10^{-4}. Our observations pave the way for expanding the application of TMD-based FETs to diode rectification devices, along with optoelectronic applications.

Graphene, which is one of the most intriguing two-dimensional (2D) materials for electronic applications due to its high electron mobility, flexibility, thermal conductivity, large surface area, and impermeability to gases, has been studied extensively over last two decades[1–8]. Despite its many merits for use in electronic materials, the application of graphene for switching devices is restricted due to its gapless nature in the pristine state[9]. However, transition metal dichalcogenides (TMDs), which are 2D semiconductor materials, exhibit a wide range of doping and band structure dynamics, allowing them to be used in a broad range of optoelectronics and nanoelectronics[10–13]. TMDs are composed of atomic layers bound together by van der Waals forces[14] and have good electronic transport channels with minimal scattering centers because they do not possess any interlayer covalent bonds[15,16]. Therefore, the bandgap and atomically thin layered structure of 2D TMDs render them a viable material for the active channel of field-effect transistor applications, such as ultra-fast photodetectors[17], electro- and photo-catalysis, supercapacitors[18], biosensors, energy storage devices, and memory devices, among others [19–23].

In the context of TMDs for use in electronic material applications, $MoTe_2$ has gained significant interest owing to its fascinating semiconducting, metallic, and superconducting characteristics[24–27]. The direct bandgap of $MoTe_2$ varies between 0.88 and 1.1 eV depending on the lattice configuration and number of layers[28–30]. In addition, since the bandgap of $MoTe_2$ is significantly smaller than those of MoS_2[31,32] and WSe_2[33,34], $MoTe_2$ is a good candidate for optoelectronic devices that provide a response covering the near-infrared wavelength region[35]. Moreover, in comparison to sulfur-terminated TMDs, Fermi-level pinning at the $MoTe_2$-metal interface is significantly weaker[36]. Despite the narrow energy bandgap of this material, numerous methods have been reported for band modulation and control of the charge carrier polarity[37,38]. On the other hand, hexagonal boron nitride (h-BN), an insulating 2D material, has recently attracted growing interest because of its mechanical robustness,

[1]Department of Physics and Astronomy, and Graphene Research Institute-Texas Photonics Center International Research Center (GRI–TPC IRC), Sejong University, Seoul 05006, Korea. [2]Department of Electrical Engineering, Sejong University, Seoul 05006, Korea. [3]Department of Convergence Engineering for Intelligent Drone, Sejong University, Seoul 05006, Korea. [4]These authors contributed equally: Muhammad Asghar Khan and Muhammad Farooq Khan. ✉email: eom@sejong.ac.kr

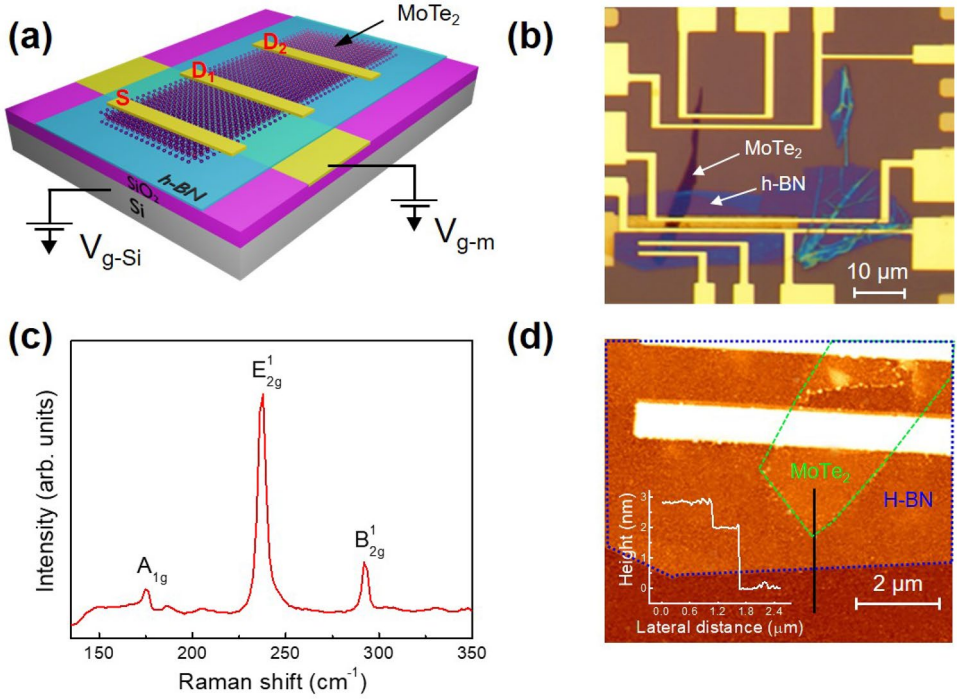

Figure 1. (**a**) Schematic diagram of an h-BN/$MoTe_2$ FET. (**b**) Optical image of an h-BN/$MoTe_2$ FET. (**c**) Raman spectrum of $MoTe_2$. (**d**) AFM image and height profile of an h-BN/$MoTe_2$ FET.

its exceptional thermal conductivity due to its strong BN covalent bonds, and its donor/acceptor-like defect states that control the doping mechanism[39,40].

It is therefore important to develop an efficient doping method for 2D TMDs to promote their application in semiconducting electronic applications. In this context, the doping of $MoTe_2$ can be categorized into two types. The first method employs local electrostatic gating, which has been used successfully to create a p–n junction by polarizing a local area where the charge carrier type is opposite to that in other parts of the $MoTe_2$ flake[41,42]. Although this technique is extremely adaptable, it is particularly volatile when gate voltage is turned off. The second method consists of atomic doping and surface modification using physical and chemical processes[43,44]. These processes permanently transform the material; however, but p-type and n-type doping are difficult to combine in the local areas of a single device. There is another way to to manupolate the carrier's type in $MoTe_2$. This method involves metal contacts engineering, which makes use of low and high work function metal electrodes[45,46]. For example, platinum, which is a high work function metal, has been used for as a source and drain contact and ambipolar $MoTe_2$ was converted into a unipolar p-type field-effect transistor (FET)[47]. However, the unipolar n-type transport of $MoTe_2$ is exceedingly difficult to accomplish owing to Fermi-level pinning and a limited variety of low work function metals. Thus, to modulate the carrier type and concentration in $MoTe_2$, the development of a stable, nonvolatile, and controlled technique is necessary to adjust the properties of $MoTe_2$ from the broad perspective of electronic devices.

Here, we present a promising strategy to address the aforementioned difficulties. More specifically, we employ a localized metal gate on a specific region of $MoTe_2$, wherein h-BN is used as a dielectric material in the metal gate, and its thickness plays a vital role in the electrostatic doping of $MoTe_2$. One region of the $MoTe_2$ is placed on an h-BN substrate with a localized metal gate underneath, while the other region is placed on h-BN without a gate to allow control of the gate effect on a specific region of the $MoTe_2$. Subsequently, illumination with deep ultraviolet (DUV) light is carried out to induce charge transfer to the defect states of h-BN with the localized metal gate underneath. Then, h-BN with charged defect states functions as a gate electrode to cause electrostatic doping of the localized $MoTe_2$ region. We also investigate the characteristics of p–n diodes consisting of p-$MoTe_2$ and n-$MoTe_2$, which are fabricated using h-BN and a metal gate.

Results and discussion

Photo-induced doping effect of h-BN/$MoTe_2$ FET. h-BN and $MoTe_2$ nanoflakes were fabricated using adhesive tape and a conventional mechanical exfoliation process, and the dry transfer technique was used to prepare stacks of the h-BN/$MoTe_2$ heterostructures. Figure 1a,b show a schematic diagram and an optical microscope image of the h-BN/$MoTe_2$ heterostructure-based FET, respectively. We also examined the 2D flakes using Raman spectroscopy, which is a non-destructive and precise technique for determining the strain effect, thermal conductivity, band structure, and adsorption of chemicals on material surfaces[48–50]. To prevent the heating effect, the Raman spectra were recorded at room temperature using a laser with a wavelength of 514 nm and a low laser power of 1.0 mW. Figure 1c shows the Raman spectra of $MoTe_2$ and three peaks assigned to A_{1g} (174.63/cm),

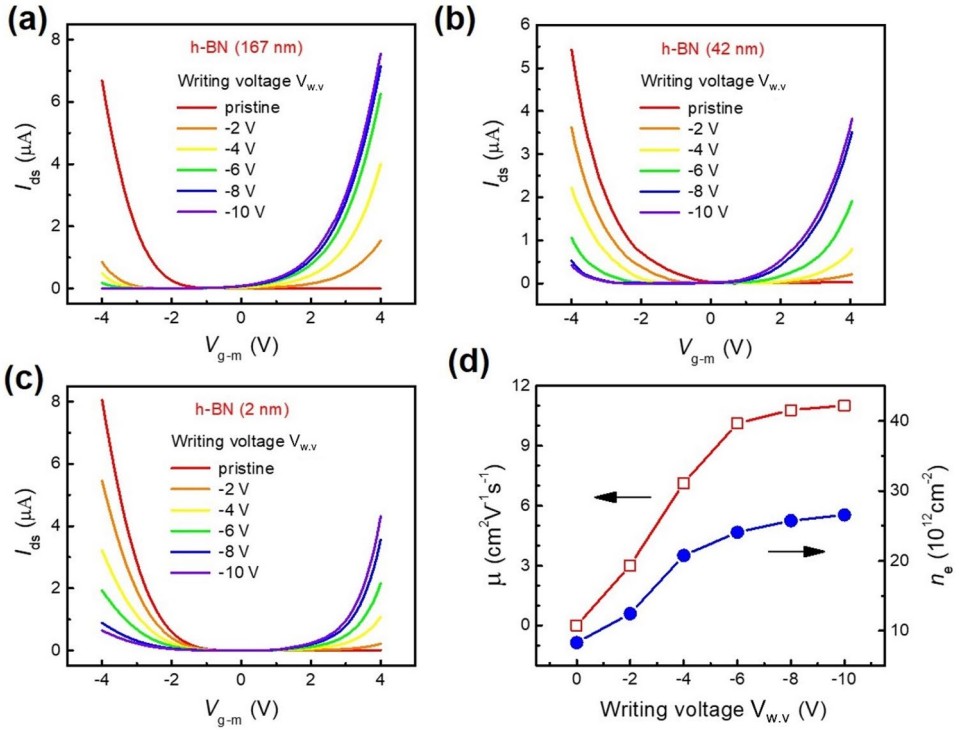

Figure 2. (**a**) Transfer characteristics of $MoTe_2$ (0.8 nm) FET on a 167 nm-thick h-BN substrate before and after photo-induced doping under DUV illumination (5 min) with writing voltages ranging from – 2 to – 10 V. (**b**) Transfer characteristics of the $MoTe_2$ (2.4 nm) FET on a 42 nm-thick h-BN substrate. (**c**) Transfer characteristics of the thin $MoTe_2$ (1.6 nm) FET on a 2 nm-thick h-BN substrate. (**d**) Electron mobility and carrier concentration of the $MoTe_2$ (0.8 nm) FET on a 167 nm-thick h-BN substrate after photo-induced doping with different metal gate voltages.

E^1_{2g} (237.87/cm), and B^1_{2g} (291.97/cm). The Raman spectra of h-BN are provided in supplementary information Fig. S1, where we observed a dominant E_{2g} peak (1364.47/cm). Figure 1d shows the topographical atomic force microscopy (AFM) image and height profile of the h-BN/$MoTe_2$ heterostructure, indicating that the thicknesses of the h-BN and $MoTe_2$ components were 2 and 0.8 nm, respectively.

The charge carrier type of a TMD plays an important role in the interface resistance between the contact metal and semiconductor. Pristine $MoTe_2$ can be either ambipolar or unipolar, being n-type or p-type, depending on its natural doping state[36,51–56]. We found that our thin $MoTe_2$ flakes were p-type in the pristine state. Thus, we initially fabricated a thin layer of $MoTe_2$ (0.8 nm) on a thick h-BN layer (167 nm). A Si/SiO_2 substrate was employed, where Si was degenerately doped for use as the back gate. The AFM images and height profiles of both h-BN and $MoTe_2$ are shown in supplementary information Fig. S2. Pristine $MoTe_2$ (0.8 nm) was found to exhibit p-type behavior, as shown in the transfer curves ($I_{ds-}V_{g-m}$) and ($I_{ds}-V_{g-Si}$) given in Fig. 2a and supplementary information Fig. S3a, respectively. During the transfer curve measurements, which were performed in a vacuum, the drain-source voltage (V_{ds}) was fixed at 0.5 V. In addition, we have investigated the output characteristics of pristine thin p-type $MoTe_2$ and found that I–V curves are nonlinear as shown in Fig. S3b, which indicates the existence of a Schottky barrier between thin $MoTe_2$ and metal contact (Cr/Au). Subsequently, the photo-induced doping effect was investigated when h-BN/$MoTe_2$ was illuminated by DUV for various time intervals with the application of a writing voltage ($V_{w.v}$) ranging from – 2 to – 10 V, as shown in Fig. 2a. The writing voltages are applied through a localized metal gate (Cr/Au, 3/13 nm) to fill or deplete electrons in the defect sites of the h-BN layer with the help of a DUV in a vacuum. To achieve this photo-induced doping effect, the use of both a DUV and a writing voltage are essential[57]. Figure 2a shows a pristine $MoTe_2$ FET on h-BN that was initially p-type, but that had been converted into n-type by DUV illumination and the application of a writing voltage. Initially, the application of – 2 V writing voltage under DUV light illumination resulted in a change in the polarity of the pristine $MoTe_2$ from p-type to n-type, as shown in Fig. 2a. Upon further increasing the writing voltage, the $MoTe_2$ region above the localized metal gate became completely n-type at a – 10 V writing voltage[58–60]. In addition, higher writing voltages resulted in more positive charges on the h-BN flake, which eventually provided an additional positive gate voltage. This photo-induced doping effect of $MoTe_2$ can be attributed to a mechanism involving the electron depletion of donor-like defects in the h-BN flakes, which are generated by the negative gate voltage upon DUV optical excitement[61,62]. The depleted electrons enter the conduction band of the h-BN and then transfer to the $MoTe_2$, leaving positively ionized defects inside the h-BN layer, which can be observed under an external electric field (V_{g-m}). Consequently, these positively charged donor-like defects in the h-BN resulted in the electrostatic doping effect of $MoTe_2$.

Effect of the h-BN thickness. To investigate whether donor-like defects exist at the h-BN/$MoTe_2$ interface or inside the h-BN itself, we measured the photo-induced doping characteristics of $MoTe_2$ films with various h-BN thicknesses. If the photo-induced doping rate is proportional to the h-BN thickness, then it can be assumed that the defects exist inside the h-BN body; however, if the photo-induced doping effect originates from defects at the interface, it must be independent of the h-BN thickness. Thus, we fabricated thin (0.8–2.4 nm) $MoTe_2$ FETs with different h-BN thicknesses to reveal the role of the h-BN thickness in the photo-induced doping effect. The transfer characteristics of the $MoTe_2$ (2.4 nm)/h-BN(42 nm) heterostructure were measured with a drain-source voltage of 0.5 V and a metal gate voltage from − 4 to + 4 V as shown in Fig. 2b. AFM confirmed the thicknesses of the $MoTe_2$ and h-BN layers, as shown in supplementary information Fig. S4. As the writing voltage was increased from − 2 to − 10 V, the polarity of $MoTe_2$ changed from p-type towards n-type, but it did not convert completely to n-type, remaining ambipolar. Similarly, the transfer characteristics of another $MoTe_2$ (1.6 nm thickness) FET on a thin (2 nm) h-BN layer were evaluated and are shown in Fig. 2c. In this case, we also observed that the p-type pristine $MoTe_2$ did not completely change its polarity to n-type and again remained ambipolar. The photo-induced doping effect rates in Fig. 2b,c are in contrast to those in Fig. 2a, where the underlying h-BN flakes are particularly thick. Our findings therefore imply that photo-induced doping in h-BN/$MoTe_2$ heterostructures is attributed to the optical stimulation of electronic states within the h-BN layer, and the thickness of this h-BN layer plays an important role in determining the extent of photo-induced doping. It is also possible that donor-like defect states may exist at different depths inside the h-BN flakes; Fig. S5 in supplementary information shows a schematic representation of the remaining positive defects in thin and thick h-BN layers after DUV illumination with the application of a writing voltage. Since DUV is illuminated from the top side of the h-BN flake, the positive defects are found more in the upper part of the h-BN flake. To compare the photo-induced doping effect at different writing voltages, we estimated the carrier density of the $MoTe_2$ FET. The charge-carrier concentration (n_e) can be calculated as follows[63]:

$$n_e = \frac{C_g\left(V_{g-m} - V_{th}\right)}{e},$$

where V_{th} is the electron transport threshold voltage, V_{g-m} is the metal gate voltage, and e is the charge of an electron (1.602×10^{-19} C). The capacitance value (C_g) of h-BN per unit area can be calculated as $C_g = \varepsilon_0\, \varepsilon_r/d$, where d is the thickness of the h-BN layer, ε_0 is the vacuum permittivity, and ε_r is the dielectric constant of h-BN. Figure S6a in supplementary information shows the gate capacitance vs frequency graphs for different thicknesses of h-BN, which demonstrates that the capacitance decreases with an increasing h-BN layer thickness as shown in Fig. S6b. Figure 2d shows the electron carrier concentration n_e after photo-induced doping under the application of a writing voltage ($V_{w.v}$) in combination with DUV for a $MoTe_2$ (0.8 nm) FET on a thick (167 nm) h-BN layer. The carrier concentration (n_e) was estimated at $V_{g-m} = +4$ V after photo-induced doping. Similarly, we estimated n_e at $V_{g-m} = 0$ V as shown in Fig. S6c, which shows a similar behaviour but the number of charge carriers is less as compared to n_e at $V_{g-m} = +4$ V. In addition, we calculated the field-effect mobility of the $MoTe_2$ FET using the following equation.

$$\mu = \frac{L}{W}\left(\frac{dI_{ds}}{dV_{g-m}}\right)\frac{1}{C_g V_{ds}}$$

where W is the channel width, L is the channel length, and $\frac{dI_{ds}}{dV_{g-m}}$ represents the slope of the linear part of the transfer characteristics of the $MoTe_2$ FET at an applied V_{ds} of 0.5 V. Figure 2d shows the mobility of the $MoTe_2$ (0.8 nm) FET on a thick (167 nm) h-BN layer after the application of a writing voltage $V_{w.v}$ in combination with DUV. Furthermore, the photo-induced doping effect was found to be stable for several days. The $MoTe_2$ FET demonstrated a stable n-type doping effect as shown in supplementary information Fig. S7a.

Effect of the $MoTe_2$ thickness. We also investigated the dependence of the $MoTe_2$ flake on the photo-induced doping effect. For this purpose, two different thicknesses of $MoTe_2$ flakes were placed on an h-BN layer, and the transfer curves were measured after photo-induced doping with various writing voltages. Figure 3a shows the transfer curves of the $MoTe_2$ (6.4 nm) FET on h-BN (160 nm), which exhibits ambipolar behavior in the pristine state. Further, we have examined the output characteristics of pristine thick n-type $MoTe_2$ and found that I–V curves are nonlinear as shown in Fig. S8. However, the writing voltage was increased from − 2 to − 10 V, the n-type characteristics of the $MoTe_2$ FET were enhanced after photo-induced doping. For comparison, we examined the photo-induced doping effect in a thicker $MoTe_2$ (46 nm) FET on h-BN (165 nm), as shown in Fig. 3b. The transfer curve indicated the n-type characteristics of the pristine $MoTe_2$ FET, and it was observed that the photo-induced doping treatment enhanced the n-type properties. More specifically, the pristine $MoTe_2$ flake exhibited p-type characteristics when its thickness was < 2.4 nm, as shown in Fig. 2a–c, whereas the thick (46 nm) $MoTe_2$ flake exhibited n-type characteristics in the pristine state. These results indicate that a p–n junction can be formed in thin $MoTe_2$ flakes using a combination of photo-induced doping treatment and a local metal gate.

$MoTe_2$ p–n diodes with different h-BN thicknesses. Subsequently, we employed the photo-induced doping technique to prepare n-type regions at local regions of thin $MoTe_2$ flakes (0.8–2.4 nm thick) on h-BN mounted on metal gates, while the other regions remained p-type, similar to the pristine state of $MoTe_2$. Although the DUV illuminated the entire area of the h-BN layer, only the donor-like defects at the local regions over the metal gate could be charged. Consequently, a p–n diode was obtained in the $MoTe_2$ flake between terminals *S*

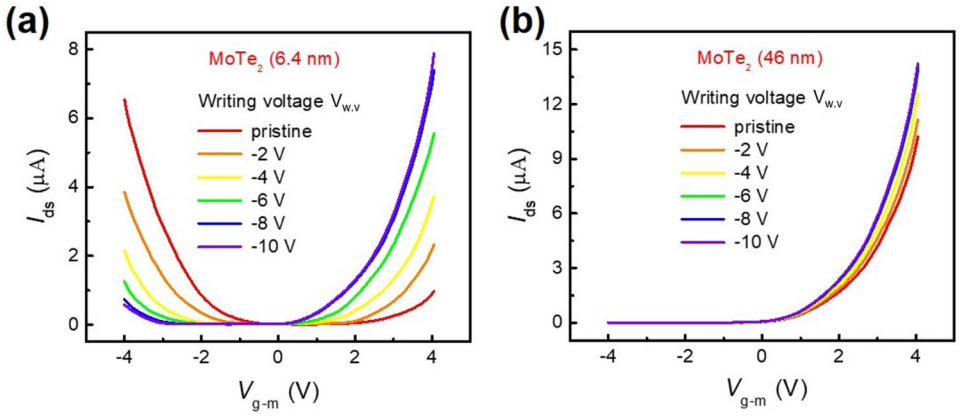

Figure 3. (**a**) Transfer characteristics of the $MoTe_2$ (6.4 nm) FET on a 160 nm-thick h-BN substrate. (**b**) Transfer characteristics of the $MoTe_2$ (46 nm) FET on a 165 nm-thick h-BN substrate.

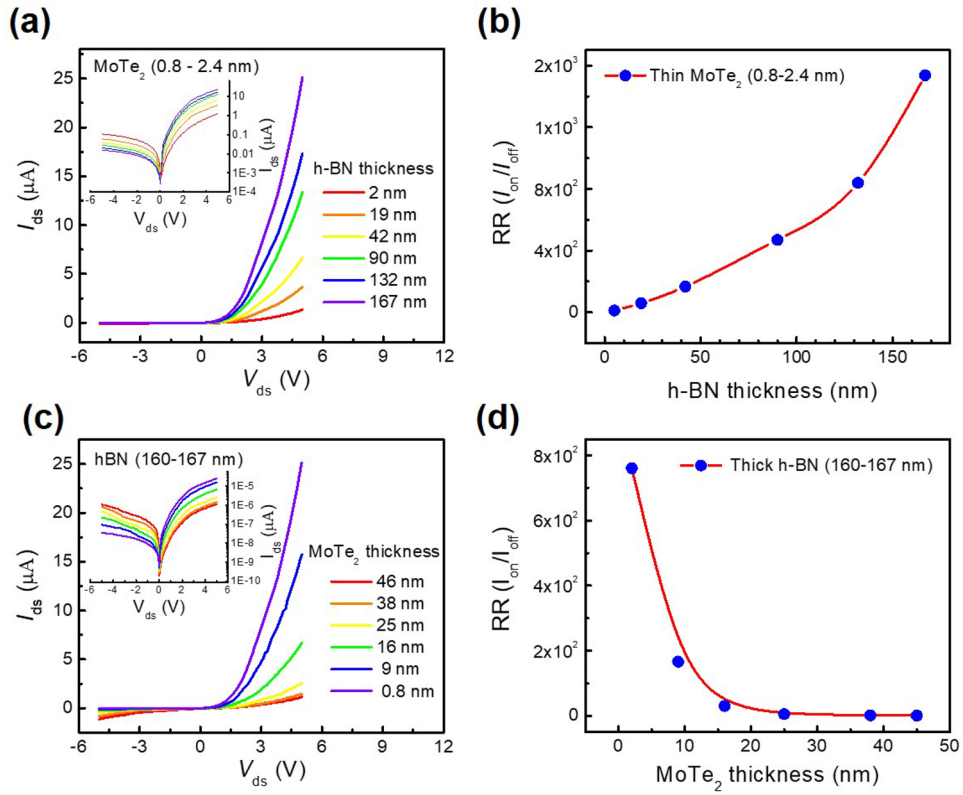

Figure 4. (**a**) Output characteristics of the $MoTe_2$ p–n diodes on h-BN substrates of different thicknesses, where the thicknesses of the $MoTe_2$ flakes ranged from 0.8 to 2.4 nm. (**b**) Rectification ratio of the $MoTe_2$ p–n diodes on h-BN substrates of different thicknesses, where the thicknesses of the $MoTe_2$ flakes ranged from 0.8 to 2.4 nm. (**c**) Output characteristics of the $MoTe_2$ p–n diodes for $MoTe_2$ flakes of different thicknesses. (**d**) Rectification ratio of the $MoTe_2$ p–n diodes for $MoTe_2$ flakes of different thicknesses, where the thicknesses of the h-BN flakes ranged from 160 to 167 nm.

and D_2, as shown in Fig. 1a. In addition, Fig. 4a shows the output characteristics of the $MoTe_2$ p–n diodes with different h-BN thicknesses after photo-induced doping; the inset of Fig. 4a shows the log scale $I_{ds} - V_{ds}$ curves, indicating the rectification characteristics. Since the photo-induced doping rate of $MoTe_2$ depends on the thickness of the h-BN layer (see Fig. 2), the function of the p–n diode is expected to also be dependent on this thickness. Figure 4b shows the rectification ratio (RR) of the $MoTe_2$ p–n diode for different h-BN thicknesses, where the RR is defined by I_{on} at $V_{ds} = +5$ V divided by I_{off} at $V_{ds} = -5$ V. The highest RR value ($\sim 1.5 \times 10^3$) was found for the $MoTe_2$ flake mounted on the thickest h-BN layer (167 nm). We also investigated the $MoTe_2$ p–n diode char-

acteristics for different thicknesses of $MoTe_2$ flakes. Thus, Fig. 4c shows the output characteristics of the $MoTe_2$ p–n diodes with various thicknesses of $MoTe_2$, and the inset shows the I_{ds}–V_{ds} curves on a logarithmic scale. As expected, diode characteristics were generally not observed in $MoTe_2$ flakes with thicknesses > 16 nm due to the fact that the majority of the flakes will be in the n-type state (i.e., that of the pristine state). As shown in Fig. 4d, a higher RR was achieved for thinner $MoTe_2$ flakes.

Following our examination of the photo-induced doping effect with a negative writing voltage of the metal gate, which mainly relies on the presence of donor-like defects in the h-BN layer, we moved on to address the possibility of reverse photo-induced doping. For this purpose, a $MoTe_2$ (0.8 nm) FET on an h-BN layer (167 nm) was subjected to DUV illumination for 5 min with a positive writing voltage for the metal gate, as shown in supplementary information Fig. S7b. The same system was used in combination with a writing voltage of − 10 V before starting the experiment, and reverse photo-induced doping was investigated with positive writing voltages ranging from + 2 to + 10 V. It was found that the transfer curve changed toward p-type as the writing voltage increased, but it remained more like n-type even with the highest writing voltage of + 10 V. It should also be noted here that the density of acceptor-like defects was lower than that of the donor-like defect states in the h-BN layer.

Materials and methods

Fabrication of $MoTe_2$ field-effect transistors on h-BN. The natural bulk crystals of h-BN and $MoTe_2$ were provided by HQ graphene. Using adhesive tape in a cleanroom environment, the mechanical exfoliation method was used to obtain ultrathin nanoflakes of h-BN and $MoTe_2$ from their bulk forms. A photoresist (SPR) and ethyl lactate (EL) were spin-coated onto Si/SiO_2 (SiO_2: 300 nm) substrates in the initial stage of the photolithography process. Subsequently, the obtained patterns were exposed to oxygen plasma for 5 min to eliminate the SPR and EL residues. A thermal evaporator was then used to evaporate Cr/Au (3/30 nm) for the large patterns, while the bottom electrode composed of Cr/Au (3/13 nm) was fabricated using conventional e-beam lithography and thermal evaporation techniques. Subsequently, a large h-BN flake was dry-transferred onto the top of the bottom electrode, while the other remainder was present on the Si/SiO_2 substrate. The $MoTe_2$ flake was then transferred onto the h-BN layer using a micromanipulator, as shown in Fig. S9 in supplementary information. At the end of the transfer procedure, the substrate was placed on a hot plate at 90 °C to eliminate vapor from the external surfaces and interfaces. After each transfer process, the samples were cleaned with acetone and methanol, and finally dried under a flow of N_2 gas. The source/drain electrodes were fabricated using conventional e-beam lithography. Finally, Cr/Au (10/80 nm) metal contacts were deposited using a thermal evaporation technique.

Photo-induced doping and measurements. For the photo-induced doping treatment, the $MoTe_2$ FETs on h-BN were illuminated by DUV light (λ = 220 nm, 11 mW cm^{-2}). Optical microscopy and Raman spectroscopy were used to examine the $MoTe_2$ flakes, and their thicknesses were measured by AFM. The electrical transport properties were measured in a vacuum using a source meter (Keithley 2400) and a picoammeter (Keithley 6485).

Conclusion

We herein reported the fabrication of $MoTe_2$ field-effect transistors (FETs) on hexagonal boron nitride (h-BN) with a localized metal gate and found that the photo-induced doping treatment was most effective for thinner $MoTe_2$ flakes mounted on a thicker h-BN layer. The use of a negative writing voltage under deep-ultraviolet (DUV) illumination induced n-doping of the $MoTe_2$ FET, while the use of a positive writing voltage under DUV illumination induced p-doping; this difference was attributed to the donor- and accepter-like defects present in the h-BN. In addition, it was found that the photo-induced doping effect became stronger as the writing voltage was increased. Furthermore, a negative writing voltage resulted in a stronger doping effect than a positive writing voltage, which indicates that donor-like defects are more dominant than acceptor-like defects in the h-BN. These observations clearly demonstrate the success of this selectable local doping technique, which is applicable as a post-fabrication treatment method.

Data availability

The data that support the findings of this study are available upon reasonable request from the corresponding author.

Received: 18 May 2022; Accepted: 7 July 2022
Published online: 15 July 2022

References

1. Afroj, S., Tan, S., Abdelkader, A. M., Novoselov, K. S. & Karim, N. Highly conductive, scalable, and machine washable graphene-based e-textiles for multifunctional wearable electronic applications. *Adv. Funct. Mater.* **30**, 2000293 (2020).
2. Geim, A. K. & Novoselov, K. S. The rise of graphene. *Nat. Mater.* **6**, 183–191 (2007).
3. Novoselov, K. S. *et al.* A roadmap for graphene. *Nature* **490**, 192–200 (2012).
4. Iqbal, M. Z. & Faisal, M. M. Fowler-Nordheim tunneling characteristics of graphene/hBN/metal heterojunctions. *J. Appl. Phys.* **125**, 084902 (2019).
5. De Fazio, D. *et al.* High responsivity, large-area graphene/MoS2 flexible photodetectors. *ACS Nano* **10**, 8252–8262 (2016).
6. Bae, S. *et al.* Roll-to-roll production of 30-inch graphene films for transparent electrodes. *Nat. Nanotechnol.* **5**, 574–578 (2010).
7. Schwierz, F. Graphene transistors. *Nat. Nanotechnol.* **5**, 487–496 (2010).
8. Kim, K. S. *et al.* Large-scale pattern growth of graphene films for stretchable transparent electrodes. *Nature* **457**, 706–710 (2009).

9. Wang, J., Van Pottelberge, R., Jacobs, A., Van Duppen, B. & Peeters, F. M. Confinement and edge effects on atomic collapse in graphene nanoribbons. *Phys. Rev. B* **103**, 035426 (2021).
10. Wang, Q. H., Kalantar-Zadeh, K., Kis, A., Coleman, J. N. & Strano, M. S. Electronics and optoelectronics of two-dimensional transition metal dichalcogenides. *Nat. Nanotechnol.* **7**, 699–712 (2012).
11. Yang, Y., Liu, Z., Shu, K., Li, L. & Li, J. Improved performances of CVD-grown MoS2 based phototransistors enabled by encapsulation. *Adv. Mater. Interfaces* **8**, 2100164 (2021).
12. Zhai, X. *et al.* Enhanced optoelectronic performance of CVD-grown metal-semiconductor NiTe2/MoS2 heterostructures. *ACS Appl. Mater. Interfaces* **12**, 24093–24101 (2020).
13. Rehman, S. *et al.* Tunable resistive switching of vertical ReSe2/graphene hetero-structure enabled by Schottky barrier height and DUV light. *J. Alloys Compd.* **855**, 157310 (2021).
14. Novoselov, K. S. *et al.* Two-dimensional atomic crystals. *Proc. Natl. Acad. Sci.* **102**, 10451–10453 (2005).
15. Chhowalla, M. *et al.* The chemistry of two-dimensional layered transition metal dichalcogenide nanosheets. *Nat. Chem.* **5**, 263–275 (2013).
16. Sundaram, R. S. *et al.* Electroluminescence in single layer MoS2. *Nano Lett.* **13**, 1416–1421 (2013).
17. Afzal, A. M., Iqbal, M. Z., Dastgeer, G., Nazir, G. & Eom, J. Ultrafast and highly stable photodetectors based on p-GeSe/n-ReSe2 heterostructures. *ACS Appl. Mater. Interfaces* **13**, 47882–47894 (2021).
18. Gowrisankar, A., Sherryn, A. L. & Selvaraju, T. In situ integrated 2D reduced graphene oxide nanosheets with MoSSe for hydrogen evolution reaction and supercapacitor application. *Appl. Surf. Sci. Adv.* **3**, 100054 (2021).
19. Wu, E. *et al.* Tunable and nonvolatile multibit data storage memory based on MoTe2/boron nitride/graphene heterostructures through contact engineering. *Nanotechnology* **31**, 485205 (2020).
20. Panda, M. R., Sarkar, A., Bao, Q. & Mitra, S. Electrochemical investigation of MoTe2/rGO composite materials for sodium-ion battery application. *AIP Conf. Proc.* **1961**, 030033 (2018).
21. Mukherjee, B. *et al.* Laser-assisted multilevel non-volatile memory device based on 2D van-der-Waals few-layer-ReS2/h-BN/Graphene heterostructures. *Adv. Funct. Mater.* **30**, 2001688 (2020).
22. Lei, S. *et al.* Optoelectronic memory using two-dimensional materials. *Nano Lett.* **15**, 259–265 (2015).
23. Rehman, S., Khan, M. F., Kim, H.-D. & Kim, S. Analog–digital hybrid computing with SnS2 memtransistor for low-powered sensor fusion. *Nat. Commun.* **13**, 1–8 (2022).
24. Keum, D. H. *et al.* Bandgap opening in few-layered monoclinic MoTe2. *Nat. Phys.* **11**, 482–486 (2015).
25. Qi, Y. *et al.* Superconductivity in Weyl semimetal candidate MoTe2. *Nat. Commun.* **7**, 11038 (2016).
26. Zhu, W. *et al.* Electronic transport and device prospects of monolayer molybdenum disulphide grown by chemical vapour deposition. *Nat. Commun.* **5**, 3087 (2014).
27. Wu, E. *et al.* Dynamically controllable polarity modulation of MoTe2 field-effect transistors through ultraviolet light and electrostatic activation. *Sci. Adv.* **5**, 3430 (2019).
28. Lezama, I. G. *et al.* Indirect-to-direct band gap crossover in few-layer MoTe2. *Nano Lett.* **15**, 2336–2342 (2015).
29. Ruppert, C., Aslan, O. B. & Heinz, T. F. Optical properties and band gap of single- and few-layer MoTe2 crystals. *Nano Lett.* **14**, 6231–6236 (2014).
30. Cho, S. *et al.* Phase patterning for ohmic homojunction contact in MoTe2. *Science* **349**, 625–628 (2015).
31. Radisavljevic, B., Radenovic, A., Brivio, J., Giacometti, V. & Kis, A. Single-layer MoS2 transistors. *Nat. Nanotechnol.* **6**, 147–150 (2011).
32. Lopez-Sanchez, O., Lembke, D., Kayci, M., Radenovic, A. & Kis, A. Ultrasensitive photodetectors based on monolayer MoS2. *Nat. Nanotechnol.* **8**, 497–501 (2013).
33. Das, S., Prakash, A., Salazar, R. & Appenzeller, J. Toward low-power electronics: Tunneling phenomena in transition metal dichalcogenides. *ACS Nano* **8**, 1681–1689 (2014).
34. Das, S. & Appenzeller, J. WSe2 field effect transistors with enhanced ambipolar characteristics. *Appl. Phys. Lett.* **103**, 103501 (2013).
35. Zhang, K. *et al.* Ultrasensitive near-infrared photodetectors based on a grapheme-MoTe2-graphene vertical van der waals heterostructure. *ACS Appl. Mater. Interfaces* **9**, 5392–5398 (2017).
36. Kim, C. *et al.* Fermi level pinning at electrical metal contacts of monolayer molybdenum dichalcogenides. *ACS Nano* **11**, 1588–1596 (2017).
37. Ali, F. *et al.* Traps at the hBN/WSe2 interface and their impact on polarity transition in WSe2. *2DMater* **8**, 035027 (2021).
38. Du, J. *et al.* Gate-controlled polarity-reversible photodiodes with ambipolar 2D semiconductors. *Adv. Funct. Mater.* **31**, 2007559 (2021).
39. Lu, Q. *et al.* Preparation of boron nitride nanoparticles with oxygen doping and a study of their room-temperature ferromagnetism. *ACS Appl. Mater. Interfaces* **10**, 12947–12953 (2018).
40. Mohsin, A. *et al.* Mapping the layer count of few-layer hexagonal boron nitride at high lateral spatial resolutions. *2DMater* **5**, 015007 (2017).
41. Nakaharai, S. *et al.* Electrostatically reversible polarity of ambipolar α-MoTe2 transistors. *ACS Nano* **9**, 5976–5983 (2015).
42. Larentis, S. *et al.* Reconfigurable complementary monolayer MoTe2 field-effect transistors for integrated circuits. *ACS Nano* **11**, 4832–4839 (2017).
43. Luo, W. *et al.* Carrier modulation of ambipolar few-layer MoTe2 transistors by MgO surface charge transfer doping. *Adv. Funct. Mater.* **28**, 1704539 (2018).
44. Chen, J. *et al.* Contact engineering of molybdenum ditelluride field effect transistors through rapid thermal annealing. *ACS Appl. Mater. Interfaces* **9**, 30107–30114 (2017).
45. Zhu, M., Luo, W., Wu, N., Zhang, X. & Qin, S. Engineering few-layer MoTe2 devices by Co/hBN tunnel contacts. *Appl. Phys. Lett.* **112**, 183102 (2018).
46. Gong, C., Colombo, L., Wallace, R. M. & Cho, K. The unusual mechanism of partial fermi level pinning at metal–MoS2 interfaces. *Nano Lett.* **14**, 1714–1720 (2014).
47. Pezeshki, A. *et al.* Static and dynamic performance of complementary inverters based on nanosheet α-MoTe2 p-channel and MoS2 n-channel transistors. *ACS Nano* **10**, 1118–1125 (2016).
48. Late, D. J. Temperature-dependent phonon shifts in atomically thin MoTe2 nanosheets. *Appl. Mater. Today* **5**, 98–102 (2016).
49. Tan, Y. *et al.* Controllable 2H-to-1T′ phase transition in few-layer MoTe2. *Nanoscale* **10**, 19964–19971 (2018).
50. Zhang, H. *et al.* High temperature Raman investigation of few-layer MoTe2. *Appl. Phys. Lett.* **108**, 091902 (2016).
51. Lin, Y.-F. *et al.* Ambipolar MoTe2 transistors and their applications in logic circuits. *Adv. Mater.* **26**, 3263–3269 (2014).
52. Mleczko, M. J. *et al.* Contact engineering high-performance n-type MoTe2 transistors. *Nano Lett.* **19**, 6352–6362 (2019).
53. Wu, E. *et al.* Specific and highly sensitive detection of ketone compounds based on p-Type MoTe2 under Ultraviolet Illumination. *ACS Appl. Mater. Interfaces* **10**, 35664–35669 (2018).
54. Ji, H. *et al.* Thickness-dependent carrier mobility of ambipolar MoTe2: Interplay between interface trap and Coulomb scattering. *Appl. Phys. Lett.* **110**, 183501 (2017).
55. Liu, Y., Stradins, P. & Wei, S. H. Van der Waals metal-semiconductor junction: Weak Fermi level pinning enables effective tuning of Schottky barrier. *Sci. Adv.* **2**, e1600069 (2016).
56. Rani, A., DiCamillo, K., Khan, M. A. H., Paranjape, M. & Zaghloul, M. E. Tuning the polarity of MoTe2 FETs by varying the channel thickness for gas-sensing applications. *Sensors* **19**, 2551 (2019).

57. Attaccalite, C., Bockstedte, M., Marini, A., Rubio, A. & Wirtz, L. Coupling of excitons and defect states in boron-nitride nanostructures. *Phys. Rev. B* **83**, 144115 (2011).
58. Ross, J. S. *et al.* Electrically tunable excitonic light-emitting diodes based on monolayer WSe2 p–n junctions. *Nat. Nanotechnol.* **9**, 268–272 (2014).
59. Huang, W. *et al.* Multibit optoelectronic memory in top-floating-gated van der waals heterostructures. *Adv. Funct. Mater.* **29**, 1902890 (2019).
60. Wu, F. *et al.* Gate-tunable negative differential resistance behaviors in a hBN-Encapsulated BP-MoS2 Heterojunction. *ACS Appl. Mater. Interfaces* **13**, 26161–26169 (2021).
61. Ju, L. *et al.* Photoinduced doping in heterostructures of graphene and boron nitride. *Nat. Nanotechnol.* **9**, 348–352 (2014).
62. Zhang, J. *et al.* UV light modulated synaptic behavior of MoTe2/BN heterostructure. *Nanotechnology* **32**, 475207 (2021).
63. Lee, Y.-H. *et al.* Synthesis and transfer of single-layer transition metal disulfides on diverse surfaces. *Nano Lett.* **13**, 1852–1857 (2013).

Acknowledgements

This work was supported by the National Research Foundation of Korea (NRF) grant funded by the Korea government(MSIT)(No. 2021R1A4A1031900 and the Global Research and Development Center Program No. 2018K1A4A3A01064272).

Author contributions

M.A.K., M.F.K. and J.E. were responsible for the experimental design and interpretation as well as writing, revision and finalisation of the manuscript. S.R., H.P., G.D. and B.M.K. performed the electrical measurement and sample charactersization.

Competing interests

The authors declare no competing interests.

Additional information

Supplementary Information The online version contains supplementary material available at https://doi.org/10.1038/s41598-022-16298-w.

Correspondence and requests for materials should be addressed to J.E.

Reprints and permissions information is available at www.nature.com/reprints.

Publisher's note Springer Nature remains neutral with regard to jurisdictional claims in published maps and institutional affiliations.